Electrodialysis with bipolar membranes to valorize saline waste streams: analysing the fate of valuable minor elements

Julio Lopez[a,b,*], Antonia Filingeri[c], Andrea Culcasi[c,*], Marc Fernández de Labastida[a,b], Alessandro Tamburini[c,d], José Luis Cortina[a,b], Giorgio Micale[c], Andrea Cipollina[c]

[a]*Chemical Engineering Department, Escola d'Enginyeria de Barcelona Est (EEBE), Universitat Politècnica de Catalunya (UPC)-BarcelonaTECH, C/ Eduard Maristany 10-14, Campus Diagonal-Besòs, 08930 Barcelona, Spain;*

[b]*Barcelona Research Center for Multiscale Science and Engineering, Campus Diagonal-Besòs, 08930 Barcelona, Spain;*

[c]*Dipartimento di Ingegneria, Università degli Studi di Palermo, viale delle Scienze ed. 6, 90128 Palermo, Italy;*

[d]*ResourSEAs SrL, Viale delle Scienze, Ed.16, 90128 Palermo, Italy.*

[*]Corresponding authors: julio.lopez.rodriguez@upc.edu, andrea.culcasi@unipa.it

Graphical abstract

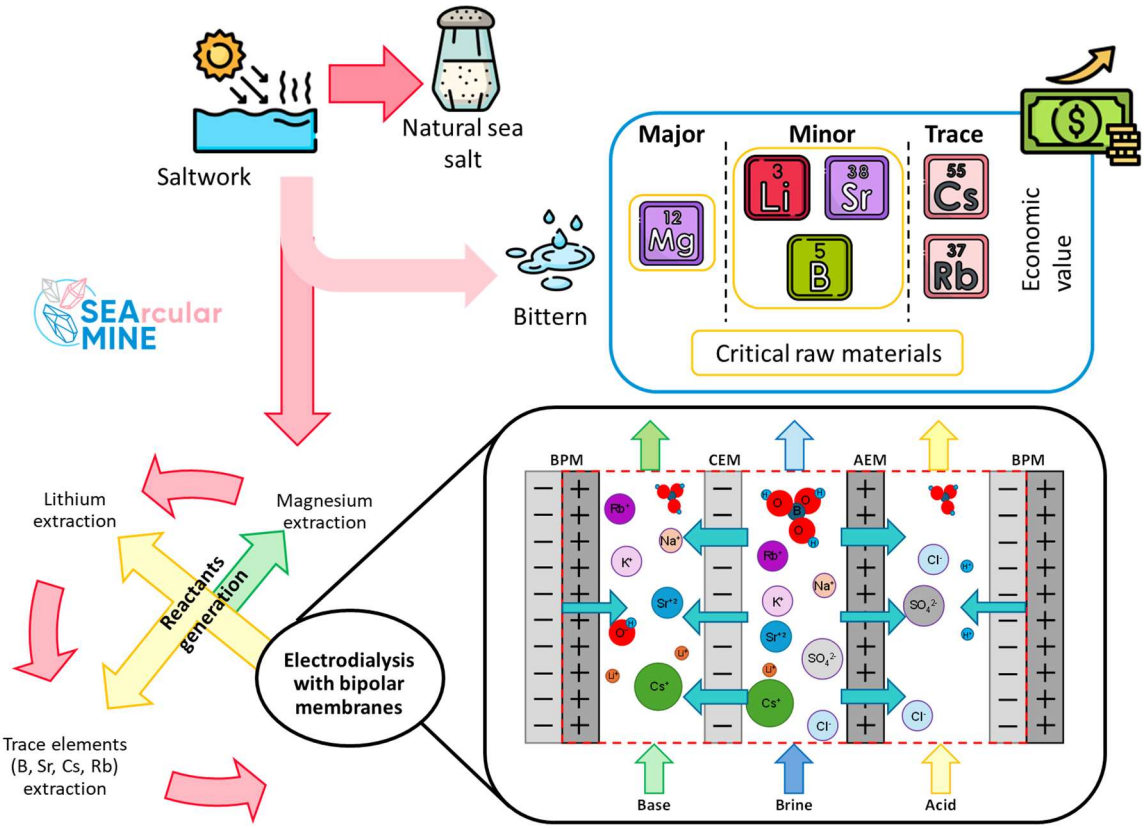

Highlights

- Saltwork real brines were tested in Electrodialysis with bipolar membrane (EDBM)
- New EDBM integration schemes in circular processes are explored
- Migration of minor and trace elements (TEs) as Li, B, Sr, Cs and Rb was assessed
- Feed brines in the base channel (Layout 2) did not affect the EDBM performance
- Cationic metals (Li^+, Rb^+, Sr^{+2} and Cs^+) were maintained in the alkaline circuit of the integrated process.
- Neutral B species ($H_3BO_3(aq)$) slightly/slowly diffused towards both acid and base compartments

Abstract

Brine mining can represent a valuable non-conventional resource for the extraction of Mg, Li, B, Sr and other Trace Elements (TEs) such as Rb, Cs, whose recoveries require chemical reagents such as alkaline and acidic solutions. In a circular strategy, these required chemicals can be produced in-situ through Electrodialysis with Bipolar Membrane (EDBM). In this work, a laboratory EDBM unit was operated using real brines from Trapani saltworks to investigate, for the first time, the migration of minor and trace ions, as Li, B, Sr, Cs and Rb through ion-exchange membranes (IEMs). Two different operating configurations were tested by feeding real brines: i) only in the salt channel or ii) in both salt and alkaline compartments. Trace ions migration was assessed by determining their apparent transport number in IEMs to better understanding their "fate" within the EDBM process.

The use of real solutions in the base channel resulted in a 50% reduction in the process water demand, while achieving similar overall Current Efficiencies (75-78%) and Specific Energy Consumptions (1.50-1.80 kWh/kg_{NaOH}) compared to the reference layout, where real brine was only fed in the salt compartment. Li, Rb, Sr and Cs were mostly transported across the cation-exchange membrane and concentrated in the alkaline channel. Such results lay the ground for the use of complex (multi-ionic) solutions and new designs of the EDBM process that can be operated in integrated chains to valorize saline wastes, reducing water consumption and avoiding the dilution of trace elements before their selective recovery.

Keywords: electro-membrane process; anion-exchange membrane; boron; lithium; rubidium; caesium; strontium

1. Introduction

The continuous need for raw materials has made it necessary to seek alternative sources, especially after the COVID-19 pandemic, which impacted supply chains and shipments, resulting in shortages and price increases (De Vet et al., 2021). During the last decades, the European Union (EU) has been implementing policies aiming to shift from traditional linear to circular economy models (European Commission, 2014). Among them, the EU has created a list of Critical Raw Materials (CRMs) that includes those of high importance for the EU economy and with a high supply risk, such as Mg, B, Co, Ge, Li and Sr, among others (European Commission, 2023). For example, China provides 93% of the EU's Mg supply, while 98% of borates used within the EU are imported from Turkey (European Commission, 2023).

Considering the lack of CRMs within the EU and the supply dependence on external countries, there is strong research interest in the possibility of obtaining such materials from non-conventional sources using circular economy approaches. Indeed, in recent years, researchers have focused on recovering critical raw materials (i.e., Mg, Li, B, Cs, Rb and Co) from both waste and seawater brines (so-called "seawater mining") (Can Sener et al., 2021; Kumar et al., 2021), such as those generated by seawater reverse osmosis (RO) desalination plants (Pramanik et al., 2020; Sharkh et al., 2022). Nevertheless, the low Technology Readiness Level (TRL) of the extraction technologies for those elements at concentration levels in the order of µg/L (e.g., Co, Ga, Ge), can make the process economically challenging (Ortiz-Albo et al., 2019; Shahmansouri et al., 2015). Another alternative for recovering CRMs from brines is the use of the *bitterns* produced in sea-salt extraction facilities (saltworks). In saltworks, seawater undergoes a natural evaporation process and flows along different basins, where the concentration and precipitation of undesired salts (e.g., calcium carbonate, calcium sulphate) takes place. Once the saturation of NaCl(s) is reached, it is precipitated in the crystallisation ponds (Vicari et al., 2022). The resulting *bittern*, with concentrations ranging from 20 to 40 times that of seawater (Vicari et al., 2022), is considered concentrated enough to be used for the recovery of CRMs. Within this context, the SEArcularMINE project (https://searcularmine.eu/) ("SEArcularMINE," n.d.) aims to recover Mg, Li, B, Sr and Trace Elements (TEs), such as Cs, Rb, Co, Ga and Ge, from exhausted *bitterns* (Battaglia et al., 2023, 2022; Saif et al., 2021; Vallès et al., 2023). Additionally, the chemicals needed are produced in-situ by using Electrodialysis with Bipolar Membranes (EDBM),

thus allowing the implementation of a fully circular process (Filingeri et al., 2024; León et al., 2022).

EDBM is an electro-membrane technology commonly used to valorize brines by desalinating them and producing acids and bases. EDBM is based on the use of repeating units (triplets) of ion-exchange membranes, namely monopolar cationic and anionic exchange membranes (CEM and AEM, respectively) and the bipolar membrane (BPM). Under the application of an electric field, water dissociation takes place at the interlayer of the BPM, producing H^+ and OH^-. Moreover, the electric field causes the cations and anions to migrate towards the cathode and anode to reach the OH^- and H^+, respectively, thus producing acidic and alkaline solutions (Campione et al., 2018; Fernandez-Gonzalez et al., 2016; Thiel et al., 2017).

The use of brines for converting salt into acid and base has been widely studied (Gazigil et al., 2022; Herrero-Gonzalez et al., 2020; Ibáñez et al., 2013; Reig et al., 2016; Yang et al., 2014). Ibáñez et al. (Ibáñez et al., 2013) studied the performance of a lab-scale EDBM unit, equipped with Ralex (AMH and CMH) and Neosepta (BP1) membranes, when treating synthetic RO brines, (without Ca and Mg). Concentrations of 0.8 mol/L H^+ and 1.0 mol/L OH^- at 1,000 A/m^2, with a Current Efficiency (CE) of 55% were reported. Similarly, Yang et al. (Yang et al., 2014) treated a RO brine from a power plant using a lab-scale unit assembled with commercial AEM and CEM (from Qianqiu Environmental Protection & Water Treatment Corporation, China) and a BPM from FUMATECH GmbH (Germany). Before treating the brine in the EDBM unit, it was pre-treated with NaOH and CO_2(g) to precipitate$Mg(OH)_2$(s) (>99.9%) and $CaCO_3$(s) (>99%) in order to avoid membrane scaling. Concentrations of 0.7 mol/L H^+ operating at 570 A/m^2, with a Specific Energy Consumption (SEC) of 9.0 kWh/kg HCl were measured, although no data on the OH^- production and acid and base purities were provided. Reig et al. (Reig et al., 2016) evaluated the valorisation of seawater RO brines, integrating nanofiltration unit to remove Ca and Mg and then, treat the permeate with Na_2CO_3 and NaOH to precipitate $CaCO_3$(s) (96% removal) and $Mg(OH)_2$(s) (99% removal). After that, the brine (52 g/L NaCl) was tested in a lab-scale unit from PcCell (64 cm^2) at 450 A/m^2, allowing to produce 0.88 mol/L HCl and 0.71 mol/L NaOH. Performance parameters, referred to NaOH, were 77% for CE and 2.58 kWh/kg NaOH for SEC. Despite the wide application of EDBM with brines, only a few works have been focused on the transport of ions when dealing with multi-ionic solutions. For example, Filingeri et al. (Filingeri et

al., 2023b) evaluated the performance of EDBM when treating synthetic brines from saltworks composed of Na_2SO_4, NaCl and KCl. As a result, it was observed that chlorides were transported up to 7 times faster than sulphates across AEMs, whereas CEMs showed a slightly higher selectivity towards K^+ than Na^+ (i.e., 1.2). Although multi-ionic solutions were used as the feed for EDBM, the analysis was focused only on the main ions present in the synthetic solution. However, the fate of trace elements is of scientific interest, especially for applications where the aim is to recover and concentrate these ions present in saline solutions. Tang et al. (Tang et al., 2023) studied the performance and ion migration of EDBM when treating RO brine to generate acids and basis. Transport of the major ions, such as Na^+, K^+, and NH_4^+, towards the base compartment (with small transport of SO_4^{2-}, Cl^- and NO_3^-) was observed. Conversely, SO_4^{2-}, Cl^- and NO_3^- migrated to the acid compartment, showing also small fractions of Na^+, K^+ and NH_4^+. Hussain et al. (Hussain et al., 2023) evaluated the effect of the main anion in solution during EDBM, observing that it was possible to reach high concentrations of acids according to the trend: $F^- > Cl^- > SO_4^{2-} > NO_3^- > PO_4^{3-} > HCO_3^-$. Recently, Filingeri et al. (Filingeri et al., 2023a) performed a long-run test with real brines from saltworks in feed and bleed configuration for 75 h, producing OH^- and H^+ concentrations of 0.44 mol/L at steady-state. However, no information of selective ions passage was provided.

In fact, notwithstanding the rising interest in application of EDBM within circular process schemes for the selective recovery of CRMs, no information has been reported so far on the transport of such elements in any of these literature works to date. This can be of crucial relevance in all cases where minor elements are targeted for their recovery within a treatment chain that includes also EDBM units for the production in-situ of acid and base solutions. In fact, it is crucial to study the transport of minor and trace elements through ion exchange membranes, in order to properly select the position of the EDBM unit in the treatment chain and avoid undesired dilution or losses of the species to be recovered. To fill this gap, this work investigates the operation of a laboratory scale EDBM unit feeding it with synthetic and real multi-ionic saline solutions. Experiments were carried out using two different layouts feeding the bittern i) only to the salt compartment and ii) both the salt and alkaline compartments. This latter configuration might offer a promising performance when integrating different technologies, as can provide a reduction on water footprint apart from capture (or concentrate) the different TEs in the alkaline loop for subsequent recovery. Initially, tests with synthetic solutions

were performed to evaluate the impact of the different configuration on acid and base production. Furthermore, experiments with real solutions containing Na^+, K^+, Cl^-, SO_4^{2-}, B, Li, Sr, Rb, Cs were conducted to examine also the migration of major, minor and trace elements through the IEMs, obtaining and comparing transport numbers for each ion.

2. Materials and methods

2.1. Solutions

Real *bitterns* coming from the Trapani saltworks (Sicily, Italy) were used as the feed solution. Due to the high solution concentration of Mg (c.a. 40 g/L) and, the lower concentration of Ca (<200 mg/L), a precipitation pre-treatment using 1.0 mol/L NaOH until reaching pH 13 was implemented to recover Mg in the form of $Mg(OH)_2$. After the sedimentation of the precipitated solid particles, the clarified solution was collected to be treated in the EDBM unit. The resulting concentration of both Ca and Mg in the clarified solutions did not exceed 10 mg/L of $CaCO_3$ equivalents, as suggested by the EDBM suppliers to prevent scaling on the membrane surface (Veolia, n.d.).

The treated solution was mainly composed of Na^+ K^+, Cl^-, SO_4^{2-} and OH^-, while other elements were present in the order of 1 mg/L (termed here "minor elements", e.g. Li, B and Sr) or 1 µg/L (termed here "trace elements", e.g. Rb, Cs). **Table 1** reports the composition of the pre-treated bittern adopted for the experiments, including major, minor and trace elements.

Table 1. Composition of the pre-treated *bittern* after the precipitation pre-treatment.

Major elements		**Minor elements**		**Trace elements**	
	g/L		mg/L		µg/L
Na^+	23.95 ± 4.99	B	28.07 ± 1.69	Rb	612.60 ± 29.35
K^+	1.45 ± 0.55	Li	1.66 ± 0.15	Cs	69.43 ± 3.54
Cl^-	17.51 ± 5.93	Sr	1.49 ± 0.07		
SO_4^{2-}	8.45 ± 0.02				
OH^-	4.25 ± 0.16				

Tests performed with real *bitterns* were compared with the experiments using synthetic solutions (see Section 2.5. *Experimental design*). To prepare the solutions, NaCl (>99.5

% purity, Saline di Volterra s.r.l., Italy, KCl (≥99% purity, SIGMA-ALDRICH) and Na_2SO_4 (ACS grade, Honeywell, USA) were used.

The acid feed solution was prepared starting from deionised water and a concentrated HCl solution (ACS Reagent 37%, Honeywell, Fluka) to reach a value of 0.05 mol/L HCl. Depending on the scenario, the alkaline stream was prepared with NaOH (micropearls, technical grade, Inovyn), being 0.05 mol/L NaOH. In all the experiments, a 0.25 mol/L Na_2SO_4 solution was used as the Electrode Rinse Solution (ERS), which was continuously recirculated in both the cathodic and anodic compartments.

2.2. Experimental set-up

The experiments were performed in an EDBM laboratory scale unit (Electromat MkI ED STACK, WTS) assembled with 5 triplets (active membrane area of 0.028 m^2). The unit also contained a cathode electrode made of platinum-coated stainless steel, and a DSA anode.

The stack was assembled with commercial membranes from WTS, being the CEM CR61N, the AEM AR103N and the BPM. Specifically, the BPM was formed by closely stacking the CR61N and a pre-treated AR103N, removing air bubbles between the two membrane layers. Both AEM and CEM are homogeneous membranes composed of aromatic cross linker casted onto thin polypropylene nonwoven cloth (SUEZ, n.d.; Zheng et al., 2006). The CR61N membrane presents sulphonic groups, while the AR103N presents quaternary ammonium functional groups (Zheng et al., 2006). The only difference between the AR103N and the pre-treated AR103N might be the presence of an immobilized metal, most likely Fe(II) (or Fe(III) or Co(II)), which promotes a lower voltage drop of water splitting at the interface of the bipolar membrane, enhancing the electrical performance (Zheng et al., 2006). The main properties of both AR103N and CR61N are shown in **Table 2**. However, no available information is provided by the supplier on the characteristics of pre-treated AR103N, nor on the performance of the BPM. Non-woven polystyrene spacers with a thickness of 760 μm were interposed between the membranes in order to form the solution channel and enhance mixing in the flowing solutions. Two overlapped spacers were included to create the ERS compartments at both the cathode and the anode. Platinum wires (127 μm of diameter, 99.9% metal basis, Alfa Aesar) were incorporated in the stack assembly to measure the voltage across the triplets, thus excluding the voltage drop in the electrode compartments,

207 due to ohmic losses and electrodic reactions, namely, hydrogen evolution at the cathode
208 and oxygen evolution at the anode.

209 **Table 2**. Main properties of the ion exchange membranes used (SUEZ, n.d.).

	AR103N	**CR61N**
Membrane thickness, μm	300	300
Ion-exchange capacity, meq/g dry membrane	2.37	2.20
Resistance in 0.1 mol/L NaCl, Ω/cm^2	2.8	3.6
Water content, %wet membrane	39	44
Burst strength, psi	95	99
Perm-selectivity, %	92	95
Water transfer, mL/F in 0.6 N NaCl at 16 mA/cm^2	115	180
Sucrose transport, g/F of 30% suc. in 0.2 N KCl at 16 mA/cm^2	3	8

210

211 The experimental set-up (see **Figure 1**) was equipped with 4 peristaltic pumps (BT601S
212 from Lead Fluid Technology, CO LTD, China) that enabled the stack to be fed with the
213 different solutions. Experiments were performed under batch configuration (feed tanks
214 with 2.0 L maximum capacity each). In order to examine the water transport between
215 compartments, the mass evolution of each feed tank was monitored using analytical scales
216 (KERN KB, Max 10,000 g, d=0.1 g). Pressure gauges (Cewal) were included in the
217 hydraulic circuit, before the entrance of the stack, to monitor the pressure drops for each
218 compartment. Both electrodes were connected to a switching mode DC power supply (BK
219 PRECISION 1902B). A digital multimeter (Fluke 175) was connected in series to the
220 electric circuit to record the applied current, while a second digital multimeter was
221 connected in parallel to periodically monitor the corresponding voltage at both electrodes
222 and platinum wires. A WTW 314i portable pH and conductivity meter was used to
223 monitor the solutions pH and conductivity evolution over time.

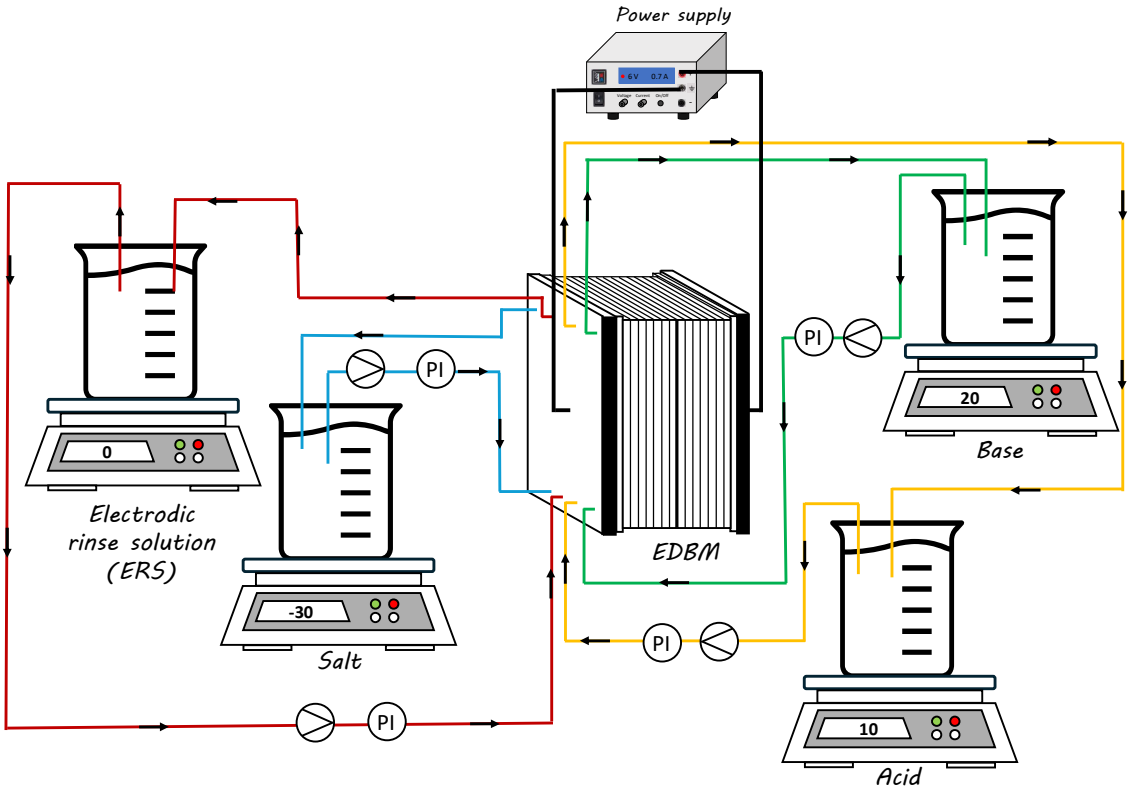

Figure 1. Schematic representation of the experimental setup, including the main auxiliary units.

2.3. Experimental procedure

After assembling the stack, (internal and external) leakage tests were performed by circulating demineralised water in all compartments for 1 hour. The mass variation in each tank was monitored, and the leakage was considered acceptable if lower than 5% (i.e. 50 mL in 1.0 L solution) per hour. In fact, according to the supplier, in this case a leakage lower than 5% is expected during operation too and can be considered negligible for the process performance. The procedure was also repeated after each test of the experimental campaign to ensure the integrity of the stack.

The experiments were carried out in batch configuration (closed-loop). Initial volumes of 1.0 L were used for the acid and base compartments, while 1.5 L was used for the salt compartment. A volume of 2.0 L was used for ERS, as in previous studies (Filingeri et al., 2024, 2023b). Initially, the solution was fed into the empty stack to remove the air bubbles. Tests were performed at fixed current density of 300 A/m^2 for a duration of ~60–90 minutes, which was found to be enough to reach the target of 1.0 mol/L OH^-. For each

test, the mass, pH and conductivity of each solution were monitored during time, while 5 mL samples were taken every ~10-20 min from each tank for the analysis.

All tests were repeated twice to verify repeatability of the stack performances, and an average deviation of ±5% was observed.

2.4. Analytical techniques

The composition of major elements (i.e., Na^+, K^+, Cl^- and SO_4^{2-}) in the samples collected was determined using ion chromatography (Dionex ICS-1000). Cations were analysed with the IONPAC®CS16 cation-exchange column, using 0.03 mol/L methane sulfonic acid as eluent, while anions were measured with the IONPAC® AS23 anion-exchange column, using a mixture of 45 mmol/L Na_2CO_3 and 0.8 mmol/L $NaHCO_3$ as eluent solution.

The composition of the minor and trace elements was determined by using Inductively Coupled Plasma with Optical Emission Spectroscopy (5100 IPC-OES, Agilent Technologies) and Inductively Coupled Plasma with Mass Spectroscopy (7800 ICP-MS, Agilent Technologies). Samples were previously diluted with 2% vol. HNO_3 and filtered through 0.22 μm filters before analysis.

The concentration of protons and hydroxide ions was measured through a volumetric titration using previously standardized 0.05 mol/L Na_2CO_3 and 0.10 mol/L HCl, with 0.1% methyl orange solution as indicator.

2.5. Experimental design

The real saltwork *bitterns* used in this work were previously pre-treated to precipitate Mg and Ca via NaOH solution addition. Two different layouts for the EDBM unit were evaluated, where the bittern was used to feed i) the salt compartment only (**Figure 2.a**) or ii) both the salt and alkaline compartments (**Figure 2.b**). This second layout has a great potential for use in circular treatment chains, where the generated alkaline solution is re-used internally in the plant, which promotes resource circularity, minimises the water footprint, and avoids the dilution of minor and trace (Vicari et al., 2024).

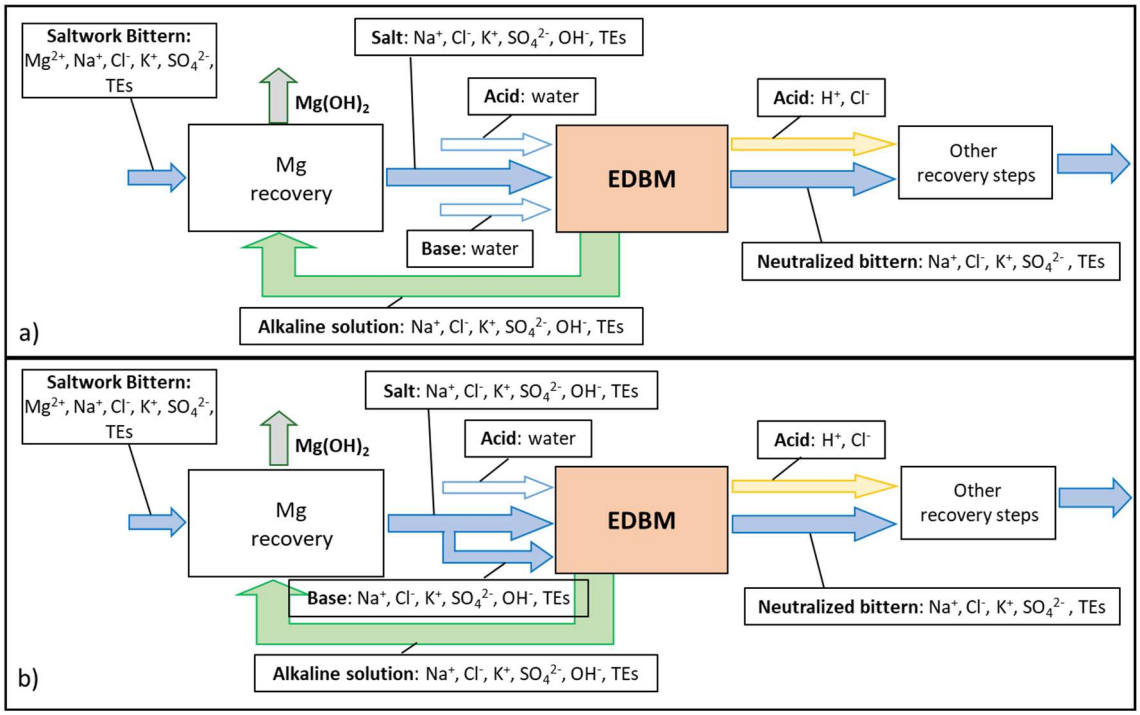

Figure 2. Treatment layouts tested in the experimental design, where the Mg, Ca-free *bittern* solution was fed to (a) the salt compartment, and (b) the salt and base compartments.

Furthermore, in the present case of bittern from saltworks, which are more concentrated in trace elements, an integrated scheme can be designed to firstly target magnesium recovery by reactive crystallisation of $Mg(OH)_2$ with NaOH, and then recover the minor and trace species ("SEArcularMINE," n.d.). In the first layout (**Figure 2.a)**, NaOH solutions with a concentration in the range of 0.5–1.0 mol/L are produced by the EDBM starting from water. However, using this layout, when this alkaline solution is mixed with a saltwork bittern to precipitate magnesium (around 40 g/L), a dilution factor of 5–10 times is obtained. This dilution reduces the concentration of the salty stream entering the EDBM unit (because of the recirculation of the base solution to the magnesium crystallizer), especially in terms of the concentration of the minor and trace elements, which are to be recovered in the following process steps. Conversely, if the saline solution exiting from the Mg recovery step is directly fed to both the alkaline and salt compartments of the EDBM system (second layout, **Figure 2.b**), the reuse of the alkaline stream in the crystallisation step would generate no dilution of minor and trace elements at steady-state operation, thus enhancing the feasibility of their recovery. Worth mentioning how the second layout also leads to a 50% reduction in water footprint of the overall process, as it avoids the use of water to feed the base compartment (where the brine is fed, instead). It should be highlighted that the internal configuration of the stack

remained the same in both layouts. The two above-mentioned layouts were already tested by Filingeri et al. (Filingeri et al., 2024) but only with 2 mol/L NaCl synthetic solutions to assess the EDBM performance when feeding a salt solution in the alkaline channel. Conversely, the aim of the present work is to investigate the fate of valuable trace and minor elements within the integrated process scheme using EDBM for the generation of reactants in situ. For this reason, tests were performed with real brines (see the composition in **Table 1**) and the results were also compared with tests performed with i) a simple NaCl solution (2 mol/L) and ii) synthetic solution mimicking the real *bittern* (1.18 mol/L Na^+, 0.91 mol/L Cl^-, 0.14 mol/L SO_4^{2-}, 0.06 mol/L K^+ and 0.05 mol/L OH^-). It should be highlighted that synthetic solutions did not contain trace and minor elements.

The acidic compartment was always fed with an initial solution at 0.05 mol/L HCl. Regarding the base channel, an initial solution at 0.05 mol/L NaOH was used in the case of the first scenario (**Figure 2.a**), or the saline feed in the case of the second scenario (**Figure 2.b**). The initial 0.05 mol/L concentrations were used to reduce the electric solution resistance during the first part of the test. The tests were performed at a mean channel flow velocity of 7 cm/s, as suggested by the manufacturer. **Table 3** reports the summary of the experimental campaign considering the different feed solutions and layouts.

Table 3. Experimental design containing the solutions used and the different layouts.

#	Layout	Salt channel	Base channel	Acid channel
Synthetic NaCl solution tests	1	2.0 mol/L NaCl	0.05 mol/L NaOH	0.05 mol/L HCl
	2	2.0 mol/L NaCl	2.0 mol/L NaCl	
Synthetic multi-ionic solution tests	1	Synthetic multi-ionic brine	0.05 mol/L NaOH	0.05 mol/L HCl
	2	Synthetic multi-ionic brine	Synthetic multi-ionic brine	
Real brine tests	1	Real brine	0.05 mol/L NaOH	0.05 mol/L HCl
	2	Real brine	Real brine	

2.6. EDBM performance indicators

In order to assess the performance of the EDBM unit, some specific indicators were calculated from the collected experimental data. Performance indicators were related to the production of NaOH, which is more valuable compared to the HCl produced (Herrero-Gonzalez and Ibañez, 2022).

The Current Efficiency (*CE*) indicates the amount of electrical current (expressed as %) effectively converted into produce OH^- in the alkaline compartment:

$$CE(\%) = \frac{\left(C_{NaOH,\tau} \cdot V_{NaOH,\tau} - C_{NaOH,0} \cdot V_{NaOH,0}\right) \cdot z \cdot F}{I \cdot N \cdot \tau} \cdot 100\% \quad (1)$$

where C_{NaOH} and V_{NaOH} refer to the concentration (mol/L) and volume (L) of NaOH solution, *F* is the Faraday constant (96,485 C/mol), *z* is the ion valence, *I* is the applied current (A), *N* is the number of triplets of the EDBM unit, and τ is the operational time (s). Subscripts τ and 0 indicate the generic and initial values of time, respectively.

The Specific Energy Consumption (*SEC*) reports the energy needed to produce 1.0 kg of NaOH, and it can be calculated according to Eq. 2:

$$SEC = \frac{I \cdot \int_0^{\tau} U_{Pt\ wires} \cdot d\tau}{3.6 \cdot 10^3 \cdot \left(C_{NaOH,\tau} \cdot V_{NaOH,\tau} - C_{NaOH,0} \cdot V_{NaOH,0}\right) \cdot M_{NaOH}} \quad (2)$$

where $U_{Pt\ wires}$ is the external voltage measured at the Pt wires (V) and M_{NaOH} is the molecular weight of NaOH (40 g/mol).

2.7. Ion transport across ion-exchange membranes

This work aims to describe the "fate" of trace elements, present in real solutions when treated with EDBM. More in detail, the transport of trace elements towards acid and base channels, as reported in **Figure 3**, was investigated.

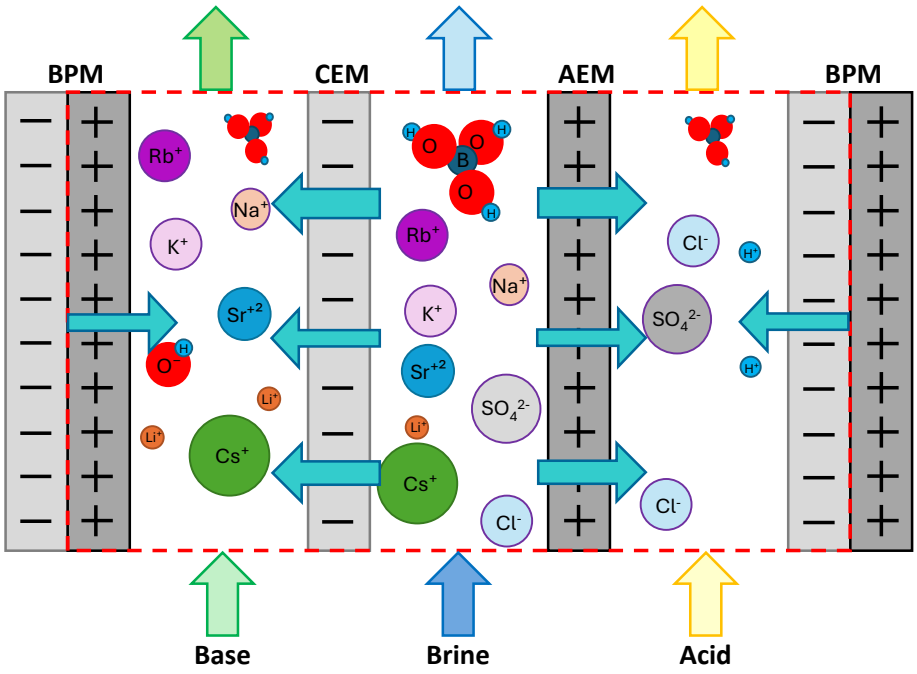

Figure 3. Schematics of ion transport from the salt compartment towards the acid and base channels

The transport of minor elements (i.e., B, Li and Sr) and TEs (i.e., Rb, Cs) was quantified in terms of fraction of the element in the specific compartment, as defined by Eq. 3:

$$\text{Element Fraction} = \frac{C_{i,\text{sol},\tau} \cdot V_{sol,\tau}}{\sum C_{i,\text{sol},0} \cdot V_{sol,0}} \quad (3)$$

where $C_{i,\text{sol},\tau}$ is the concentration of the element i in the generic solution at the generic time and $V_{sol,\tau}$ is the volume of the generic solution at a generic time. Subscript 0 refers to the beginning of the test.

The speciation of the solution was assessed using PHREEQC software (version 3.7.3) (U.S. Geological Survey, 2023) using the version of Pitzer database, modified by Vicari et al. (Vicari et al., 2022) to include also trace elements.

The procedure developed by Filingeri et al. (Filingeri et al., 2023b) was used to assess the apparent ion transport numbers across the ion-exchange membranes. **Table 4** summarizes the equations used for their determination. From the experimental data, ion fluxes across AEM and CEM were determined using Eqs. 4a and b ($J_{i,\tau}^{AEM}$ and $J_{i,\tau}^{CEM}$) for all the ions, except for OH^- and H^+. Conversely, the fluxes of H^+ and OH^- were assessed via mass balance. To determine the flux from the BPM ($J_{H^+,\tau}^{BPM}$ and $J_{OH^-,\tau}^{BPM}$ in Eq. 5) a unitary

346 transport number for both ions in the BPM was considered for simplicity (Filingeri et al.,
347 2023b). Then, due to the passage of H^+ and OH^- to the salt compartment (caused by back-
348 diffusion and a non-ideal perm-selectivity of the IEMs), their fluxes across the AEM and
349 CEM ($J_{H^+,\tau}^{AEM}$ and $J_{OH^-,\tau}^{CEM}$) were determined as the difference between direct conversion of
350 the electric current in ion current in the BPM (Eq. 5) and the fluxes resulting from the
351 mass balances (see Eqs. 6a and b). Under these assumptions, the total ions flux across
352 both IEMs, can be determined using Eqs. 7a and b. Finally, the apparent transport number
353 of a generic ion *i* across a monopolar membrane can be defined as the ratio of the ion flux
354 to the total ions flux across the IEM (see Eq. 8).

355

Table 4. Equations used for the determination of apparent transport numbers (Filingeri et al., 2023b; La Cerva et al., 2019, 2018)

Ion-fluxes across the monopolar (AEM, CEM) membrane
$$J_{i,\tau}^{AEM} = \frac{\left(V_{acid,\tau} \cdot C_{i,acid,\tau} - V_{acid,\tau=0} \cdot C_{i,\mathrm{acid},\tau=0}\right)}{N\ S\ \tau} \quad (4.a)$$
$$J_{i,\tau}^{CEM} = \frac{\left(V_{base,\tau} \cdot C_{i,base,\tau} - V_{base,\tau=0} \cdot C_{i,\mathrm{base},\tau=0}\right)}{N\ S\ \tau} \quad (4.b)$$
H^+ and OH^- flux generated at the BPM
$$J_{H^+,\tau}^{BPM} = J_{OH^-,\tau}^{BPM} = \frac{I/S}{F} \quad (5)$$
H^+ and OH^- fluxes across the monopolar (AEM, CEM) membrane
$$J_{H^+,\tau}^{AEM} = J_{H^+,\tau}^{BPM} - \frac{\left(V_{acid,\tau} \cdot C_{H^+,acid,\tau} - V_{acid,\tau=0} \cdot C_{H^+,\mathrm{acid},\tau=0}\right)}{N\ S\ \tau} \quad (6.a)$$
$$J_{OH^-,\tau}^{CEM} = J_{OH^-,\tau}^{BPM} - \frac{\left(V_{base,\tau} \cdot C_{OH^-,base,\tau} - V_{base,\tau=0} \cdot C_{OH^-,\mathrm{base},\tau=0}\right)}{N\ S\ \tau} \quad (6.b)$$
Total ion-flux across the monopolar (AEM, CEM) membrane
$$J_{tot,\tau}^{AEM} = \sum_i J_{i,\tau}^{AEM} + J_{H^+,\tau}^{AEM} \quad (7.a)$$
$$J_{tot,\tau}^{CEM} = \sum_i J_{i,\tau}^{CEM} + J_{OH^-,\tau}^{CEM} \quad (7.b)$$
Apparent transport number for a (AEM, CEM) membrane
$$t_{i,IEM,t} = \frac{J_{i,\tau}^{IEM}}{J_{tot,\tau}^{IEM}} \quad (8)$$

3. Results and discussion

In this section, the trends in the concentration of H^+ and OH^- ions in the studied scenarios are first analysed. Subsequently, the transport of minor and trace ions is analysed. Finally, the energy performance parameters of the EDBM unit are calculated.

3.1. H^+ and OH^- concentration profiles along the EDBM experiments

The first results concern the profiles of H^+ and OH^- ions obtained when treating the different solutions using the two layouts. **Figure 4** shows the concentration profiles of OH^- (**Figure 4** a and c) and H^+ (**Figure 4** b and d) as functions of time for layout 1 (**Figure**

4 a and b) and layout 2 (**Figure 4** c and d). Tests were carried out until reaching a concentration of 1.0 mol/L OH^-.

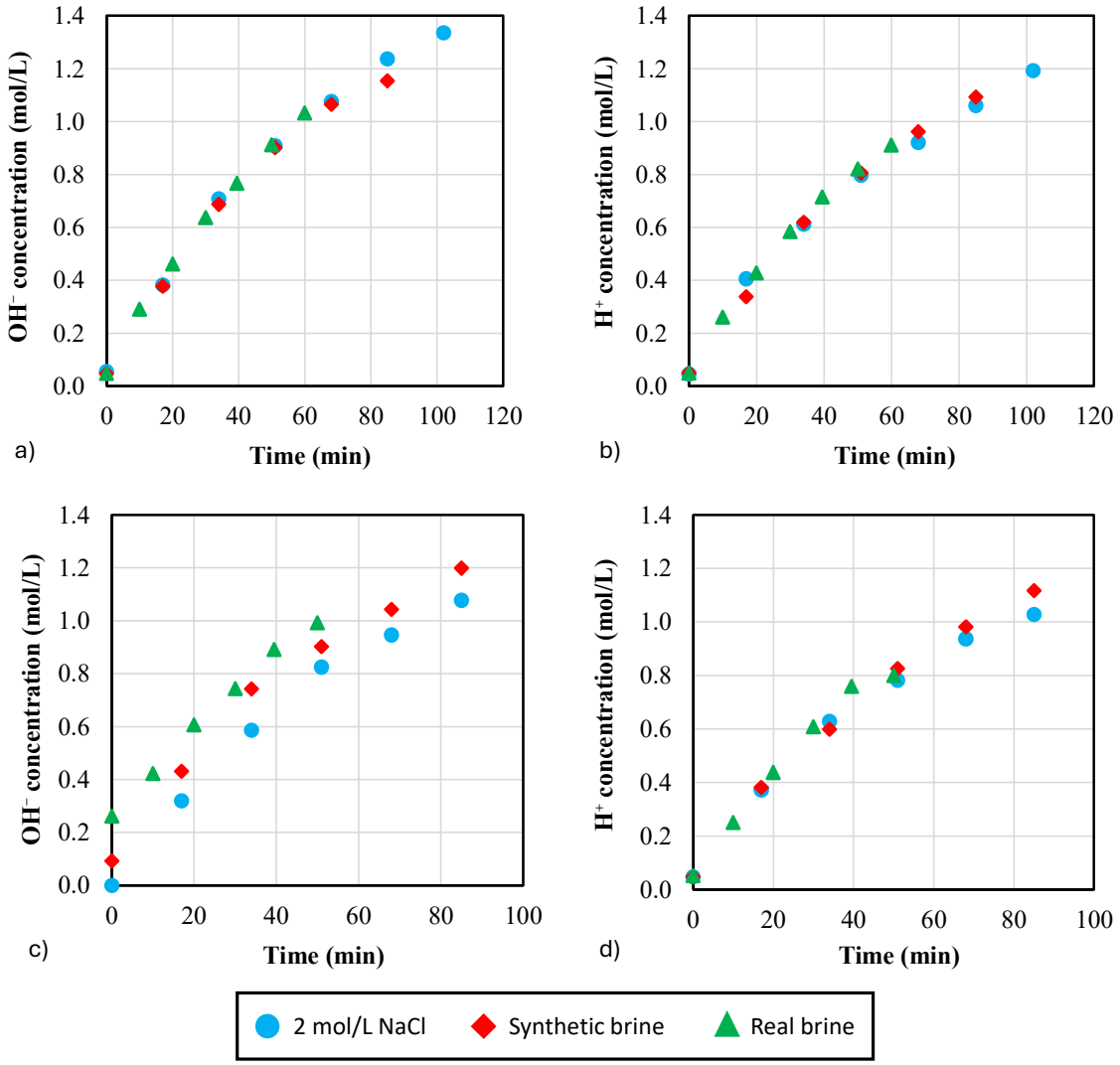

Figure 4. Concentrations of OH^- and H^+ as a function of operation time for the three tested solutions adopting the EDBM layout 1 (a,b) and layout 2 (c,d). *An average deviation between replicates of ±5% was observed.*

In all cases, the ions concentration increased over time because these tests were conducted in batch (discontinuous) mode and at a constant current density of 300 A/m^2. However, the slope of the concentration-time curve decreased over time for both OH^- and H^+, especially in the latter half of the experiments. This decrease can be attributed to non-ideal phenomena, such as diffusion, osmotic and electro-osmotic fluxes, which become increasingly significant at higher product concentrations. Notably, the use of synthetic or real solutions did not affect the trend in the alkaline and acidic concentrations, thus demonstrating that using either solution did not reduce the output of desired products.

Indeed, the OH^- targets of 0.5 mol/L and 1.0 mol/L were achieved within 23±1 min and 60±2 min, respectively, in layout 1 (see Figure 3.a). The observed discrepancy in OH^- ion concentration profiles using layout 2 (Figure 3.c) was essentially the result of the difference in the initial concentration. Specifically, in the experiments conducted using the real brine, the initial OH^- concentration was 0.26 mol/L. In contrast, the synthetic solution was prepared with a pH of 13, corresponding to an OH^- concentration of 0.1 mol/L. Indeed, if the concentration profile for the synthetic solution were adjusted by a shift of 0.16 mol/L to account for the lower initial concentration, the profiles for the real and synthetic solutions would align, thus demonstrating that the initial concentration is the key variable influencing the observed differences. The different OH- concentration profiles observed for synthetic versus real solutions in layout 2 (see **Figure 4** c) could also partially be related to the different base mass variation trends (reported in the Supplementary Material, **Figure S1**) observed when feeding a different saline solution into the base. This behaviour can be explained by the varying impact of non-ideal fluxes (e.g., diffusive and osmotic) when using a different saline stream. Furthermore, higher water transport towards the base compartment was noted when using layout 2 (see **Figure S1**), mainly related to osmosis. Comparing the concentration profiles observed for layout 1 (see **Figure 4** a) and layout 2 (see **Figure 4** c), the higher concentration measured for layout 2 can be explained mainly by the different initial concentration of OH^-. In fact, the trend in OH^- moles produced in the base channel (see **Figure S2**) was similar for both layouts and for the different salt solutions, thus highlighting similar EDBM acid/base productivity across the configurations. Importantly, this result highlights that the use of either a synthetic or real saline solution has no negative impact on the base concentration profile. Additionally, using layout 2 would allow the implementation of treatment processes in which the TEs can be concentrated rather than diluted. Indeed, this concentration process would not be possible using layout 1 due to the water being the feed the base solution in the EDBM.

For both layouts, the H^+ concentrations were lower than the OH^- concentrations (see **Figures 4 b** and **d**). Indeed, for all the tests performed, the salt compartment was found to acidify, thus meaning net proton leakage from the acid to the salt channels occurred. This difference in membrane transport can be explained qualitatively based on the known transport mechanisms in the solution phase. Indeed, the smaller size and higher mobility in solution of H^+ ions (0.282 nm and $9.31 \cdot 10^{-9}$ m^2/s) compared to OH^- (0.300 nm and

414 $5.27 \cdot 10^{-9}$ m^2/s) (Vanýsek, 1996) may result in higher mobilities also in the membrane
415 phase.

416 The results obtained in the present work are in line with the published data available in
417 the literature. Indeed, similar final OH^- concentrations, between 0.8 mol/L and 1.5 mol/L,
418 were obtained in other papers, although they used different feeds, current densities and
419 volume ratios between the salt and acid/base solutions. For instance, Filingeri et al.
420 (Filingeri et al., 2023b) obtained OH- concentrations up to 1.44 mol/L working with high-
421 concentrated brines at 300 A/m^2. Ibáñez et al. (Ibáñez et al., 2013) were able to reach 1.0
422 mol/L OH^- when treating a polished RO concentrate working at 1000 A/m^2, whereas
423 under the same conditions it was possible to reach 3.6 mol/L OH^- working with a salt-to-
424 base volume ratio of 20:1 (Herrero-Gonzalez et al., 2020).

425

426 ### 3.2. Minor elements concentration profiles along the EDBM
427 ### experiments

428 This second section of the results is devoted to the transport of trace elements among
429 compartments, examining in particular the migration of TEs present in the real brine from
430 the salt compartment towards the other three compartments (i.e, acid, base and ERS).

431 Initially, a speciation analysis of the TEs in the solution was carried out (see **Figure 5**).
432 Considering the composition shown in **Table 1** (pH 13) and the results given by
433 speciation diagrams (built using PHREEQC (U.S. Geological Survey, 2023)), the
434 following conclusions can be made regarding the treated real brine: (i) Li, Rb and Cs are
435 completely in their cationic forms (i.e., Li^+, Rb^+, and Cs^+), while Sr is mostly present as
436 a cation (i.e., Sr^{2+}) with a small portion complexed as $SrOH^+$, $SrCl^+$ and $SrSO_4(aq)$, (ii) B
437 is present as an anion (i.e. $H_4BO_4^-$) in alkaline solution and as a neutral species in acidic
438 solution (i.e., $H_3BO_3(aq)$).

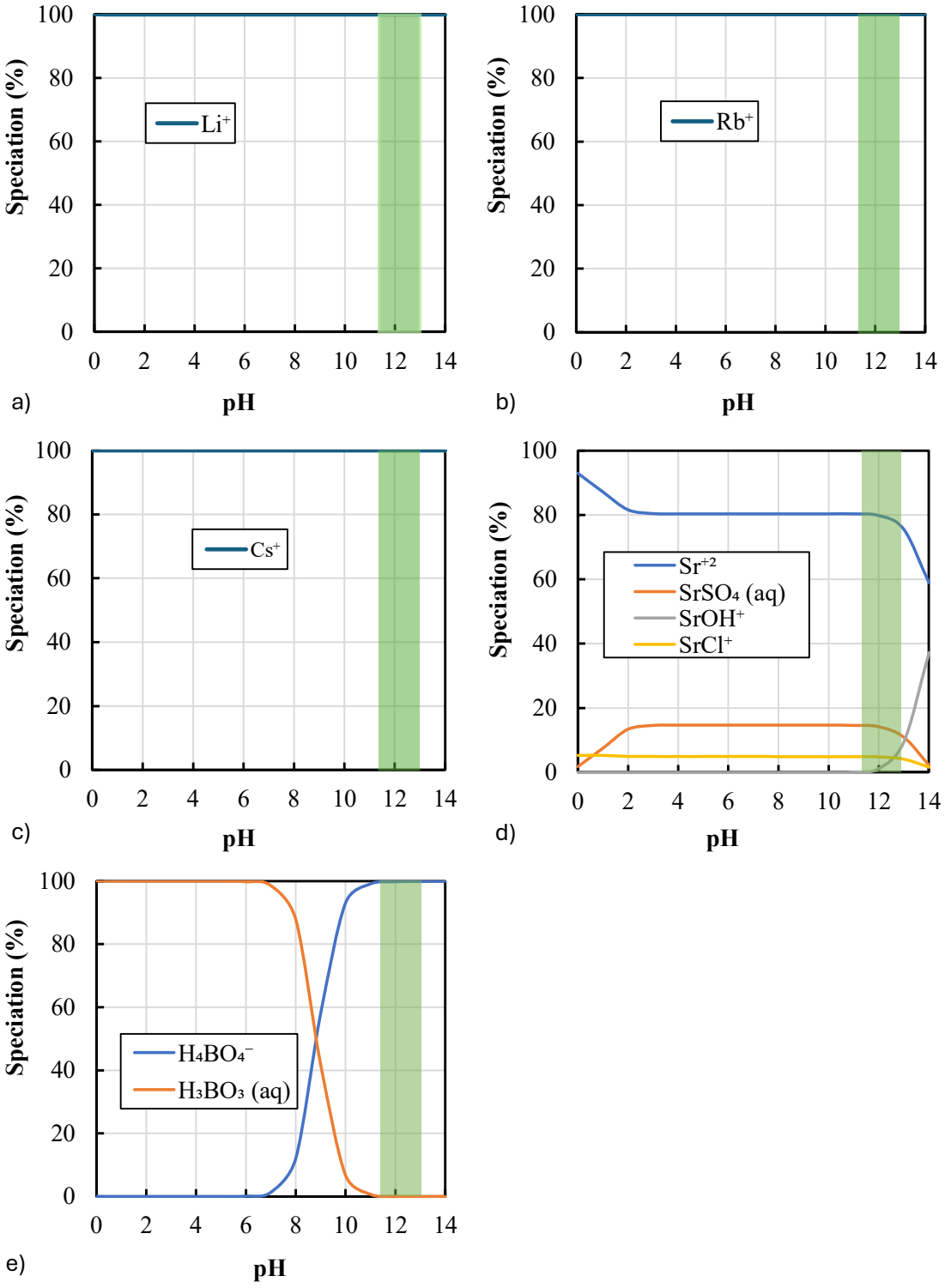

Figure 5. Speciation diagrams for (a) Li, (b) Rb, (c) Cs, (d) Sr and (e) B as a function of pH for the *bittern* after Ca and Mg removal (see **Table 1**). Diagrams were built using PHREEQC (U.S. Geological Survey, 2023).

The molar fraction of each TE in each compartment was determined by analysing samples from the four external tanks (related to the salt, acid and base solutions and ERS) at

different times during the test and is plotted in **Figure 6** for layout 1 (i.e., when brine is fed only into the salt compartment). The fractions of Li, Rb, Sr and Cs in the salt compartment tended to decrease over time in the same proportions. Most of these ions migrated towards the base compartment, whereas a small fraction was present in the ERS.

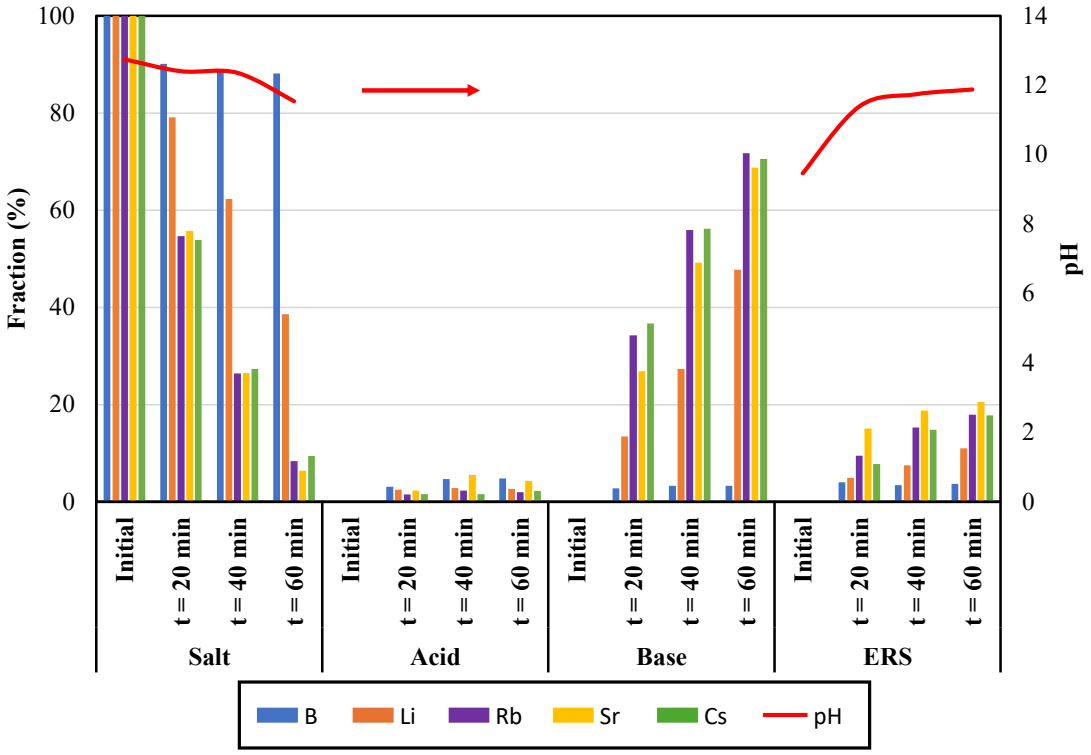

Figure 6. Molar fraction of trace elements transported from feed to the other 3 loops for the layout 1 at different sampling times

Therefore, based on their speciation (see **Figure 4**), the major cations Li^+, Rb^+, Cs^+ and Sr^{2+} moved towards the base compartment across the CEM, thus enriching the alkaline solution. TEs were also transported towards the ERS, although at a much lower rate compared to the transport towards the base. This behaviour can be attributed to the transport of TEs across the end-membrane (i.e., a CEM), which separates one salt compartment and the ERS flowing in the cathodic compartment. However, it is important to note that although this transport towards the ERS was evident at the laboratory scale due to the small number of triplets (5 in the present work), it would be negligible at the pilot and industrial scales, where tens or hundreds of triplets would be adopted. Finally, a very limited concentration reduction of B in the salt channel was observed. Indeed, the presence of B as an anionic or a neutral species (i.e., $H_4BO_4^-$ or H_3BO_3(aq), respectively) meant that it could not permeate across the CEMs and was not affected by the electric field originating inside the stack due to the applied external electric potential. Therefore,

465 the diffusive transport of boron was primarily driven by the concentration gradient
466 between the salt channel and both the acidic and alkaline compartments.

467 For comparative purposes, the fraction of TEs in the compartments for the two different
468 layouts is plotted at a time corresponding to the achievement of the target 1.0 mol/L OH^-
469 concentration (**Figure 7**). In the case of layout 2, the real brine was initially fed into both
470 the saline and alkaline tanks with volumes of 1.5 L and 1.0 L, respectively, thus meaning
471 60% of the TEs were initially fed into the salt compartment and the remaining into the
472 base compartment.

473 As a result, B remained confined within the salt and base compartments, in line with the
474 observations presented in Figure 5 for layout 1. The other TEs significantly migrated
475 towards the base compartment, with a slower passage of Li^+, as also observed for layout
476 1. Conversely, the transport of positively charged TEs towards the acidic compartment
477 was quite low (below 5% of the total TEs). This low level of transport was likely caused
478 by diffusive transport through the IEMs, as the migrative flux of the trace cations across
479 the AEMs should be significantly inhibited due to their charge and ion radius. Such
480 findings are extremely relevant in all the circular treatment chains that aims at recovering
481 critical raw materials and TEs. Indeed, this work demonstrates that the EDBM process
482 can be integrated in those chains to produce in situ the alkaline and acidic solutions,
483 instead of using external chemicals. Specifically, if the saline solutions, containing these
484 TEs, are also fed in the alkaline compartment, instead of using water as in the common
485 EDBM schemes, and then recirculated back to the previous recovery units (see **Figure**
486 **2.a**), the dilution of TEs is avoided (up to 10 times, compared to standard Mg-recovery
487 schemes for bitterns), making their subsequent separation and recovery much more
488 feasible.

489

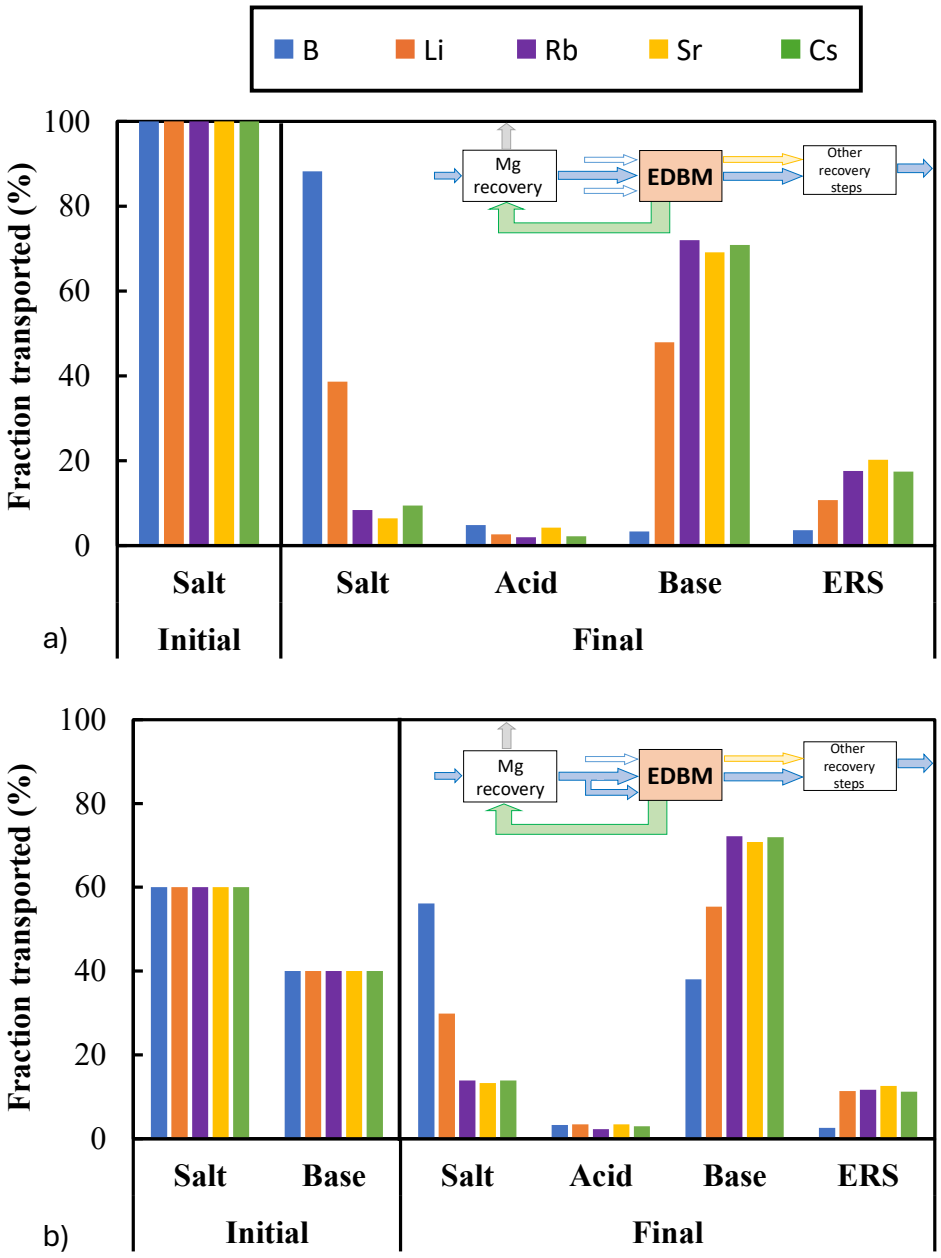

Figure 7. Fraction transported of the trace elements along the compartments for the layout 1 (a) and 2 (b).

3.3. Ions-transport characterization by transport numbers

In this section, the selective transport of the ions across the IEMs is presented. Particularly, this section of results focuses on the apparent ion transport numbers for major, minor and trace elements across the AEM and CEM, which are depicted in **Figure 8** for all ions using both layouts. The values collected refer to the time of the test at which the target concentration of 1.0 mol/L OH^- was achieved.

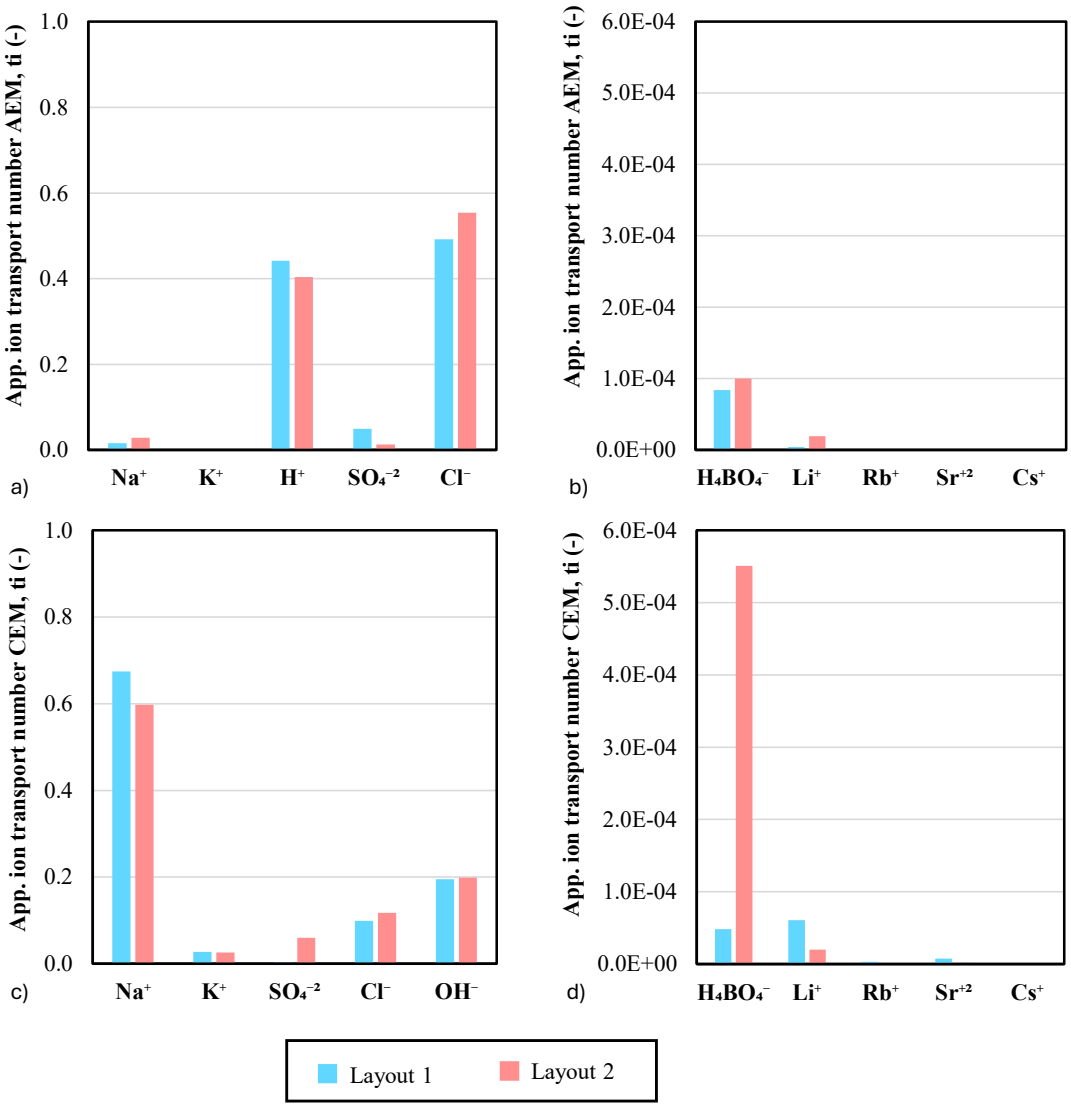

Figure 8. Apparent ion transport numbers of major, minor, and trace ions for the (a,b) AEM and (c,d) CEM.

In the case of the AEM (see **Figure 8.a-b**), it was observed that the main ion transported from the salt to the acid channel was Cl^- for both layouts, with average apparent transport numbers of 0.49 and 0.55, for layouts 1 and 2, respectively. It should be highlighted that H^+ was significantly transported across the AEM, with apparent transport number of 0.40 and 0.44, for the two layouts. Even though the positive fixed charge of the AEM, the H^+ (acting as co-ion) was able to permeate towards the salt compartment due to an ion-leakage, which outlines the low proton-blocking capacity of the tested membranes. The other ions in solution were transported to a lesser extent. This is the case for SO_4^{2-}, although the negative charge showed transport numbers of 0.01 and 0.04 due to its low mobility. Moreover, other single-charged cations were also able to permeate, mainly related to ion leakage, such as the case of Na^+ (0.01 – 0.03) and in a lesser extent of Li^+

and other TEs ($<2 \cdot 10^{-5}$). From the values obtained, it was also observed that boron permeated through the AEM with an apparent transport number value around 10^{-4}. High levels of purity in the acidic solution have been achieved in terms of the fractions of H^+ among all the cations and Cl^- among all the anions. Indeed, the results demonstrated that these fractions were 97% for H^+ and 91% for Cl^- using layout 1, while these fractions were 98% for H^+ and 95% for Cl^- using layout 2.

In the case of the CEM (see **Figure 8.c-d**), Na^+ was the ion that is being preferentially transported towards the base compartment (transport number ranging from 0.57 to 0.67, depending on the layout). Similar to the AEM case, the CEM was not able to impede completely the OH^- leakage, resulting in a transport number around 0.19. Moreover, other anions were transported across the CEM, being mainly chloride and sulphate. It should be highlighted that in this case, higher values were obtained for layout 2 than layout 1, which could be explained by a diffusive back transport from the base to the depleted salt compartment. Furthermore, despite sulphates having a high ionic radius and being negatively charged, they were found to pass across the CEM, albeit in small quantities. Finally, other cation species, were transported to a lesser extent (transport numbers below 0.02). Comparison with literature data is difficult due to the scarce availability of ion transport information in literature, such as transport numbers, that confirmed the relevance of filling this gap. Only in one of our previous studies (Filingeri et al., 2023b) the apparent transport numbers were determined when testing the SUEZ membranes with synthetic multi-ionic solutions. Similar range of values were obtained for the major and minor elements transport across both AEM and CEM but no TEs were present in the synthetic solutions.

3.4. EDBM Performance parameters

This final section aims to analyse the EDBM performance indicators, namely current efficiency (CE) and Specific Energy Consumption (SEC). **Figure 9** reports the profiles of CE (graph a) and SEC (graph b) as functions of time for layouts 1 and 2.

CE reduced over time from values between 80% and 90% until reaching a minimum around 60% at the end of the test. This behaviour is due to non-ideal phenomena, such as retro-diffusion of OH^- and H^+ from base/acid to the other compartments, osmotic and electro-osmotic fluxes, but also a partial use of electric current to transport Na^+ or Cl^- across the bipolar membranes (Culcasi et al., 2022; Filingeri et al., 2023b), especially

when Na^+ and Cl^- are present from the beginning of the experiments, as seen in layout 2. The water and other ions diffusion were enhanced as the concentration of generated acid and base increased, thus resulting in a faster reduction of the CE in the second part of the test. Interestingly, the CE trend was not affected by the use of either synthetic or real solutions. In fact, the performance of the mixed solutions, synthetic or real, showed similar or better CE than the test conducted with only NaCl in the feed. Furthermore, using the brine solution also in the alkaline compartment did not affect the efficiency of the unit.

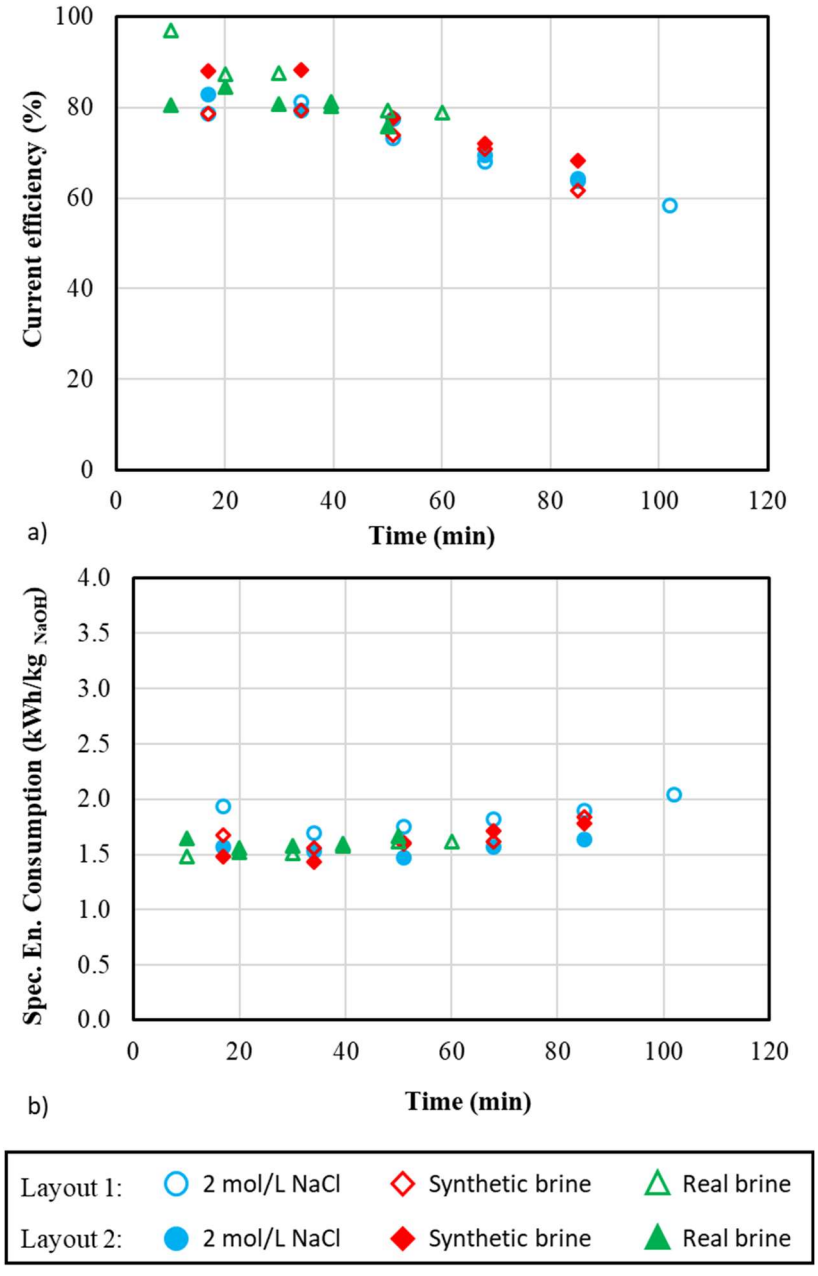

Figure 9. (a) Current Efficiency and (b) Specific Energy Consumption as a function of operation time for the three tested solutions using both layouts.

Figure 9b reports SEC referred to the alkaline product, as it is the high-added value component of the process. SEC remained almost constant/slightly increasing in the first part of the test, whereas it increased more in the second part. This behaviour can be related to the CE and voltage evolution over time (reported in **Figure S3** of the Appendix). The almost constant trend in the SEC in the first half of the test is related to the slow decrease in the CE, balanced by the similar decrease in the voltage trend, which is mainly due to the reduction in the internal electric resistance of the EDBM stack. In the second part of the test, the voltage remained constant while the CE decreased, resulting in a further increase in SEC. As already observed for CE, SEC was not affected by the use of a mixed-salts solution, synthetic or real, nor by the two different operational layouts.

In this work, similar values for CE (75-78%) and SEC (1.50-1.80 kWh/kg NaOH) were attained for both layouts at 1 mol/L OH^-. Similar values of CE (76–80% for Fumatech and 70–71% for SUEZ membranes) were reported in a previous study (Filingeri et al., 2024) when testing both layouts with 2 mol/L NaCl feed solutions. Contrary, the SEC consumptions were slightly higher when using layout 1 (1.23 kWh/kg NaOH and 1.73 kWh/kg NaOH for Fumatech and SUEZ membranes, respectively) in front of layout 2 (1.35 kWh/kg NaOH and 1.60 kWh/kg NaOH for Fumatech and SUEZ membranes, respectively). Ibáñez et al. (Ibáñez et al., 2013) reported CE values around 60% working at 1,000 A/m^2 after reaching 1.0 mol/L OH^-, without providing data on SEC. Tang et al. (Tang et al., 2023) reported SEC values of 2.7 kWh/kg NaOH and CE values of 59% after reaching 0.8 mol/L OH^- working at 24 V and a volume ratio salt to acid and alkali of 5:1.Herrero-González et al. (Herrero-Gonzalez et al., 2020), after reaching 3.6 mol/L NaOH working at 1000 A/m^2 and a volume ratio of 20:1, obtained a SEC of 43.50 kWh/kg HCl. Filingeri et al. (Filingeri et al., 2023b) when reported CE values of 75-80% and SEC values of 1.60-1.94 kWh/kg NaOH at the target of 1.0 mol/L OH^- working with synthetic solutions.

The present study confirmed how EDBM appears to be a robust technology for the treatment of real solutions, containing more ions than the typical NaCl, and can be used in alternative configurations (i.e., layout 2), where the saline solution is also fed into the alkaline compartment, showing very competitive SEC and CE, compared to previous studies. Indeed, the presence of TEs or minor elements did not appreciably alter the performance of the EDBM unit. The experimental results suggest that the TEs do not pass through the AEMs and their presence in the salt compartment (as in layout 1) or in the

salt and base compartments (as in layout 2) does not alter the performance of the EDBM unit. Results highlighted the relevance of EDBM for implementing circular schemes, especially in the case that both acidic and basic solutions are reused internally, which can lead to a lower freshwater consumption and a concentration of TEs for sub-sequent recovery.

4. Conclusions

In this study, a laboratory-scale EDBM unit was examined to investigate the transport of elements present in large and trace quantities between the acid, base, salt, and ERS compartments using both synthetic and real feed solutions. The findings indicate that the presence of trace elements, such as B, Li, Sr, Cs and Rb, in the EDBM input solutions do not significantly alter the generation of acid and base as well as CE and SEC.

Trace elements such as Li, Rb, Sr and Cs were mostly transported across the CEM (50-70 %) from the salt to the alkaline compartment. Conversely, these ions were mostly excluded by the AEM and, thus, their passage from the salt to the acid compartment was inhibited. Although a small proportion of these ions, <5%, still passed through the AEM, presumably by diffusive mechanisms given the non-ideality of the membranes. Boron is an exception since, being a negative-neutral species, depending on the pH, it crosses both the CEM and the AEM in similar amounts, thus passing into both the base and acid channels when subjected to a concentration gradient. The trends in ion transport were qualitatively similar in the two layouts studied.

Overall, this research demonstrates that the recovery of trace elements from real bitterns via circular schemes integrating the EDBM process can be enhanced by the use of optimised layouts where a “saline and TEs-enriched” solution is used to generate an alkaline stream in EDBM, to be continuously recirculated, thus maintaining very high level of concentration of all TEs to guarantee subsequent effective recovery. In addition, the proposed EDBM layout can significantly reduce the process water footprint, thus further pushing the overall process sustainability.

Acknowledgements

This work was supported by the EU within SEArcularMINE (Circular Processing of Seawater Brines from Saltworks for Recovery of Valuable Raw Materials) project – Horizon 2020 programme, Grant Agreement No. 869467. This output reflects only the

author's view. The European Health and Digital Executive Agency (HaDEA) and the European Commission cannot be held responsible for any use that may be made of the information contained therein. The work of J. López was supported within the scope of Margarita Salas fellowship, financed by the Ministerio de Universidades (Spain) and European Union – NextGenerationEU. Moreover, J.L. Cortina received support for the research through the "ICREA Academia" recognition for excellence in research funded by the Generalitat de Catalunya.

References

Battaglia, G., Berkemeyer, L., Cipollina, A., Cortina, J.L., Fernandez de Labastida, M., Lopez Rodriguez, J., Winter, D., 2022. Recovery of Lithium Carbonate from Dilute Li-Rich Brine via Homogenous and Heterogeneous Precipitation. Ind. Eng. Chem. Res. 61, 13589–13602. https://doi.org/10.1021/acs.iecr.2c01397

Battaglia, G., Domina, M.A., Lo Brutto, R., Lopez Rodriguez, J., Fernandez de Labastida, M., Cortina, J.L., Pettignano, A., Cipollina, A., Tamburini, A., Micale, G., 2023. Evaluation of the Purity of Magnesium Hydroxide Recovered from Saltwork Bitterns. Water (Switzerland) 15. https://doi.org/10.3390/w15010029

Campione, A., Gurreri, L., Ciofalo, M., Micale, G., Tamburini, A., Cipollina, A., 2018. Electrodialysis for water desalination: A critical assessment of recent developments on process fundamentals, models and applications. Desalination 434, 121–160. https://doi.org/10.1016/j.desal.2017.12.044

Can Sener, S.E., Thomas, V.M., Hogan, D.E., Maier, R.M., Carbajales-Dale, M., Barton, M.D., Karanfil, T., Crittenden, J.C., Amy, G.L., 2021. Recovery of Critical Metals from Aqueous Sources. ACS Sustain. Chem. Eng. https://doi.org/10.1021/acssuschemeng.1c03005

Culcasi, A., Gurreri, L., Tamburini, A., Lockhart Bogle, I.D., Micale, G., 2022. A Bi-objective Optimization Study of an Acid-Base Flow Battery for High Efficiency and Improved Power Density. Chem. Eng. Trans. 96, 133–138. https://doi.org/10.3303/CET2296023

De Vet, J.M., Nigohosyan, D., Nuñez Ferrer, J., Gross, A.-K., Kuehl, S., Flickenschild, M., 2021. Impacts of the COVID-19 pandemic on EU industries.

649 European Commission, 2023. Critical raw materials | Internal Market, Industry,
650 Entrepreneurship and SMEs [WWW Document].

651 European Commission, 2014. Communication from the Commission - Towards a circular
652 economy: A zero waste programme for Europe, COM.

653 Fernandez-Gonzalez, C., Dominguez-Ramos, A., Ibañez, R., Irabien, A., 2016.
654 Electrodialysis with Bipolar Membranes for Valorization of Brines. Sep. Purif. Rev.
655 45, 275–287. https://doi.org/10.1080/15422119.2015.1128951

656 Filingeri, A., Culcasi, A., Mueller, S., Lopez, J., Tamburini, A., Linnartz, C., Cortina,
657 J.L., Cipollina, A., Micale, G., 2023a. An Experimental Investigation of
658 Electrodialysis with Bipolar Membranes Long-Run Performances with Real
659 Solutions from Saltworks. Chem. Eng. Trans. 105, 535–540.

660 Filingeri, A., Herrero-Gonzalez, M., O'Sullivan, J., López Rodriguez, J., Culcasi, A.,
661 Tamburini, A., Cipollina, A., Ibañez, R., Ferrari, M.C., Cortina, J.L., Micale, G.,
662 2024. Acid/Base Production via Bipolar Membrane Electrodialysis: Brine Feed
663 Streams to Reduce Fresh Water Consumption. Ind. Eng. Chem. Res.
664 https://doi.org/10.1021/acs.iecr.3c03553

665 Filingeri, A., Lopez, J., Culcasi, A., Leon, T., Tamburini, A., Luis Cortina, J., Micale, G.,
666 Cipollina, A., 2023b. In-depth insights on multi-ionic transport in Electrodialysis
667 with bipolar membrane systems. Chem. Eng. J. 468, 143673.
668 https://doi.org/10.1016/j.cej.2023.143673

669 Gazigil, L., Er, E., Kestioğlu, O.E., Yonar, T., 2022. Pilot-Scale Test Results of
670 Electrodialysis Bipolar Membrane for Reverse-Osmosis Concentrate Recovery.
671 Membranes (Basel). 12. https://doi.org/10.3390/membranes12010083

672 Herrero-Gonzalez, M., Diaz-Guridi, P., Dominguez-Ramos, A., Irabien, A., Ibañez, R.,
673 2020. Highly concentrated HCl and NaOH from brines using electrodialysis with
674 bipolar membranes. Sep. Purif. Technol. 242.
675 https://doi.org/10.1016/j.seppur.2020.116785

676 Herrero-Gonzalez, M., Ibañez, R., 2022. Technical and Environmental Feasibilities of the
677 Commercial Production of NaOH from Brine by Means of an Integrated EDBM and
678 Evaporation Process. Membranes (Basel). 12, 885.
679 https://doi.org/10.3390/membranes12090885

Hussain, A., Wang, H., Fu, R., Afsar, N.U., Wang, B., Jiang, C., Wang, Y., Xu, T., 2023. Ion Transport Behavior in Bipolar Membrane Electrodialysis: Role of Anions. Ind. Eng. Chem. Res. 62, 698–707. https://doi.org/10.1021/acs.iecr.2c03812

Ibáñez, R., Pérez-González, A., Gómez, P., Urtiaga, A.M., Ortiz, I., 2013. Acid and base recovery from softened reverse osmosis (RO) brines. Experimental assessment using model concentrates. Desalination 309, 165–170. https://doi.org/10.1016/j.desal.2012.10.006

Kumar, A., Naidu, G., Fukuda, H., Du, F., Vigneswaran, S., Drioli, E., Lienhard, J.H., 2021. Metals Recovery from Seawater Desalination Brines: Technologies, Opportunities, and Challenges. ACS Sustain. Chem. Eng. https://doi.org/10.1021/acssuschemeng.1c00785

La Cerva, M., Gurreri, L., Cipollina, A., Tamburini, A., Ciofalo, M., Micale, G., 2019. Modelling and cost analysis of hybrid systems for seawater desalination: Electromembrane pre-treatments for Reverse Osmosis. Desalination 467, 175–195. https://doi.org/10.1016/j.desal.2019.06.010

La Cerva, M., Gurreri, L., Tedesco, M., Cipollina, A., Ciofalo, M., Tamburini, A., Micale, G., 2018. Determination of limiting current density and current efficiency in electrodialysis units. Desalination 445, 138–148. https://doi.org/10.1016/j.desal.2018.07.028

León, T., Abdullah Shah, S., López, J., Culcasi, A., Jofre, L., Cipollina, A., Cortina, J.L., Tamburini, A., Micale, G., 2022. Electrodialysis with Bipolar Membranes for the Generation of NaOH and HCl Solutions from Brines: An Inter-Laboratory Evaluation of Thin and Ultrathin Non-Woven Cloth-Based Ion-Exchange Membranes. Membranes (Basel). 12, 1204. https://doi.org/10.3390/membranes12121204

Ortiz-Albo, P., Torres-Ortega, S., González Prieto, M., Urtiaga, A., Ibañez, R., 2019. Techno-Economic Feasibility Analysis for Minor Elements Valorization from Desalination Concentrates. Sep. Purif. Rev. https://doi.org/10.1080/15422119.2018.1470537

Pramanik, B.K., Nghiem, L.D., Hai, F.I., 2020. Extraction of strategically important elements from brines: Constraints and opportunities. Water Res. 168, 1–13.

711 https://doi.org/10.1016/j.watres.2019.115149

712 Reig, M., Casas, S., Gibert, O., Valderrama, C., Cortina, J.L., 2016. Integration of
713 nanofiltration and bipolar electrodialysis for valorization of seawater desalination
714 brines: Production of drinking and waste water treatment chemicals. Desalination
715 382, 13–20. https://doi.org/10.1016/j.desal.2015.12.013

716 Saif, H.M., Huertas, R.M., Pawlowski, S., Crespo, J.G., Velizarov, S., 2021.
717 Development of highly selective composite polymeric membranes for Li+/Mg2+
718 separation. J. Memb. Sci. 620, 118891.
719 https://doi.org/10.1016/j.memsci.2020.118891

720 SEArcularMINE [WWW Document], n.d.

721 Shahmansouri, A., Min, J., Jin, L., Bellona, C., 2015. Feasibility of extracting valuable
722 minerals from desalination concentrate: A comprehensive literature review. J. Clean.
723 Prod. https://doi.org/10.1016/j.jclepro.2015.03.031

724 Sharkh, B.A., Al-Amoudi, A.A., Farooque, M., Fellows, C.M., Ihm, S., Lee, S., Li, S.,
725 Voutchkov, N., 2022. Seawater desalination concentrate—a new frontier for
726 sustainable mining of valuable minerals. npj Clean Water.
727 https://doi.org/10.1038/s41545-022-00153-6

728 SUEZ, n.d. Ionics* Ion Exchange Membranes. Water Technologies & Solutions. Fact
729 Sheet [WWW Document].

730 Tang, H., Wang, X., Zhao, X., Dong, Y., Xu, B., Wang, L., 2023. Ion migration
731 characteristics during the bipolar membrane electrodialysis treatment of
732 concentrated reverse osmosis brine. Desalination 561, 116660.
733 https://doi.org/10.1016/j.desal.2023.116660

734 Thiel, G.P., Kumar, A., Gómez-González, A., Lienhard, J.H., 2017. Utilization of
735 Desalination Brine for Sodium Hydroxide Production: Technologies, Engineering
736 Principles, Recovery Limits, and Future Directions. ACS Sustain. Chem. Eng.
737 https://doi.org/10.1021/acssuschemeng.7b02276

738 U.S. Geological Survey, 2023. PHREEQC Version 3.7.3.

739 Vallès, V., López, J., Fernández de Labastida, M., Gibert, O., Leskinen, A., Koivula, R.T.,
740 Cortina, J.L., 2023. Polymeric and inorganic sorbents as a green option to recover

741 critical raw materials at trace levels from sea saltwork bitterns. Green Chem.
742 https://doi.org/10.1039/D2GC02338E

743 Vanýsek, P., 1996. Ionic conductivity and diffusion at infinite dilution. CRC Handb.
744 Chem. Phys. 96, 5–98.

745 Veolia, n.d. Bipolar Electrodialysis (BPED) [WWW Document].

746 Vicari, F., López, J., Cassaro, C., Virruso, G., Culcasi, A., Vassallo, F., Battaglia, G.,
747 Filingeri, A., Tamburini, A., Cipollina, A., 2024. Procedimento Di Rimozione Di
748 Cationi Divalenti E Carbonio Inorganico Da Acque Saline Per Il Recupero Di
749 Elementi In Tracce E Relativo Impianto. Italian Patent Application n.
750 IT102024000005104.

751 Vicari, F., Randazzo, S., López, J., de Labastida, M.F., Vallès, V., Micale, G., Tamburini,
752 A., Staiti, G.D., Cortina, J.L., Cipollina, A., Fernández de Labastida, M., Vallès, V.,
753 Micale, G., Tamburini, A., D'Alì Staiti, G., Cortina, J.L., Cipollina, A., 2022.
754 Mining minerals and critical raw materials from bittern: Understanding metal ions
755 fate in saltwork ponds. Sci. Total Environ. 847.
756 https://doi.org/10.1016/j.scitotenv.2022.157544

757 Yang, Y., Gao, X., Fan, A., Fu, L., Gao, C., 2014. An innovative beneficial reuse of
758 seawater concentrate using bipolar membrane electrodialysis. J. Memb. Sci. 449,
759 119–126. https://doi.org/10.1016/j.memsci.2013.07.066

760 Zheng, Y., MacDonald, R.J., Ju, Y.A., Sims, K.J., 2006. Bipolar Membrane and Method
761 of Making Same. US 2006/0173084 A1.

762

763

Electrodialysis with bipolar membranes to valorize saline waste streams: analysing the fate of valuable minor elements

Julio Lopez[a,b,*], Antonia Filingeri[c], Andrea Culcasi[c,*], Marc Fernández de Labastida[a,b], Alessandro Tamburini[c,d], José Luis Cortina[a,b], Giorgio Micale[c], Andrea Cipollina[c]

[a]*Chemical Engineering Department, Escola d'Enginyeria de Barcelona Est (EEBE), Universitat Politècnica de Catalunya (UPC)-BarcelonaTECH, C/ Eduard Maristany 10-14, Campus Diagonal-Besòs, 08930 Barcelona, Spain;*

[b]*Barcelona Research Center for Multiscale Science and Engineering, Campus Diagonal-Besòs, 08930 Barcelona, Spain;*

[c]*Dipartimento di Ingegneria, Università degli Studi di Palermo, viale delle Scienze ed. 6, 90128 Palermo, Italy;*

[d]*ResourSEAs SrL, Viale delle Scienze, Ed.16, 90128 Palermo, Italy.*

[*]Corresponding authors: julio.lopez.rodriguez@upc.edu, andrea.culcasi@unipa.it

SUPPLEMENTARY MATERIAL

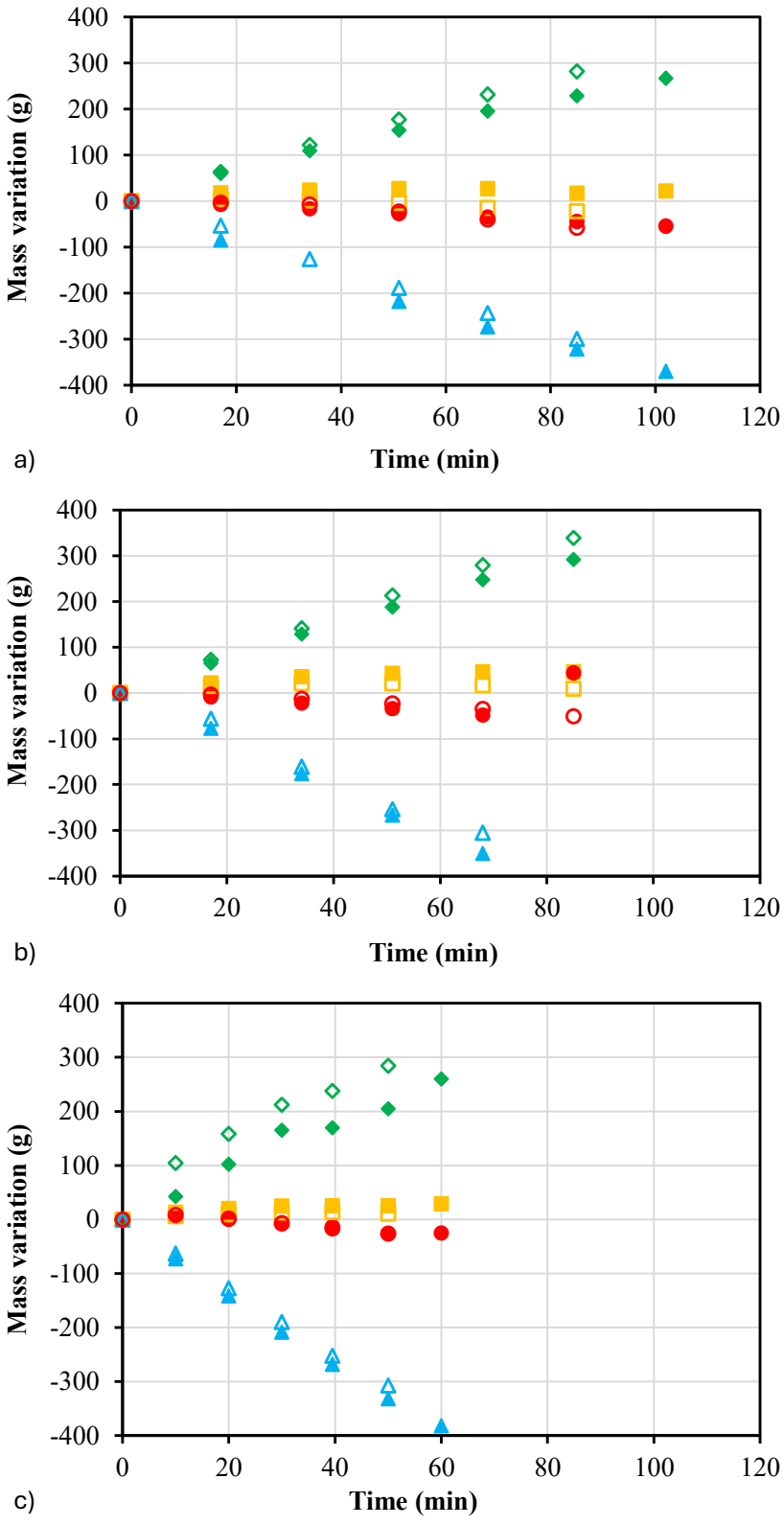

Figure S1. Mass variation in the 4 solutions as a function of operation time for (a) 2 mol/L NaCl, (b) Synthetic solution, and (c) real brine. Filled points: layout 1; empty points: layout 2. Note: mass balances are not fulfilled due to sampling.

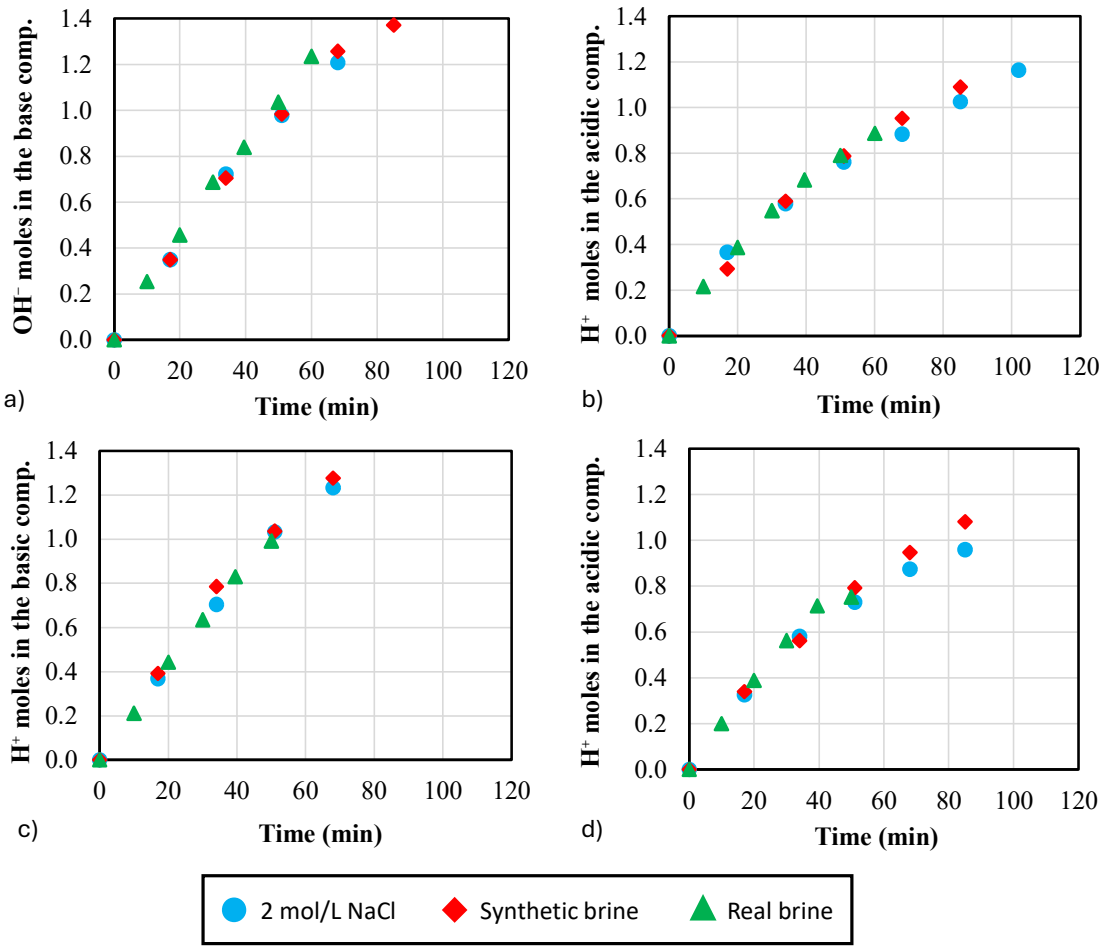

784

785

786 **Figure S2**. Moles of OH^- and H^+ in the acidic and basic compartments as a function of operation time for
787 the three tested solutions using the (a,b) layout 1 and (c,d) layout 2.

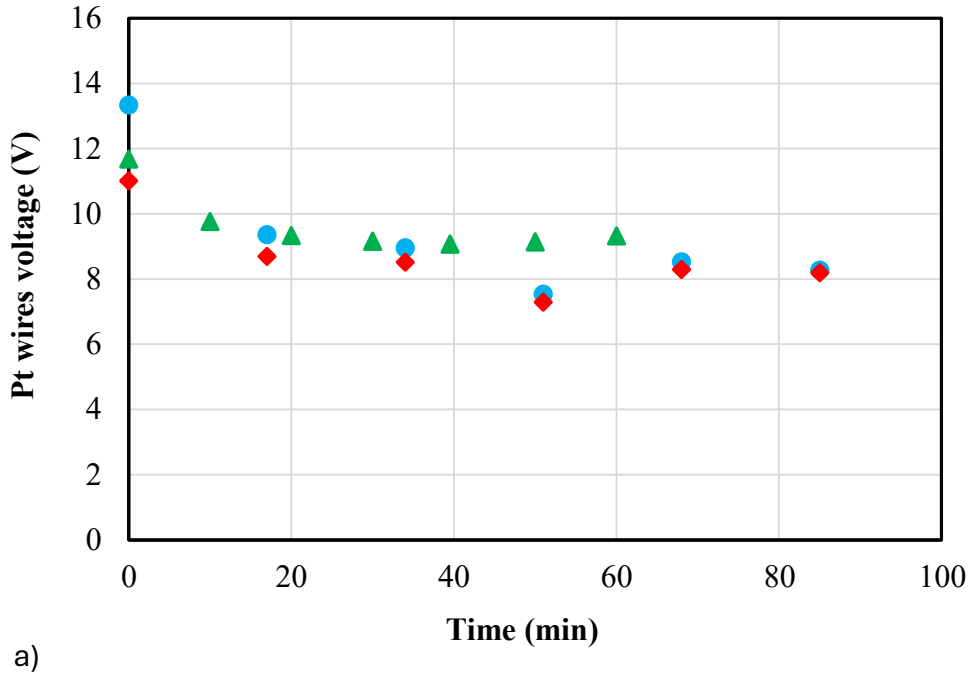

a)

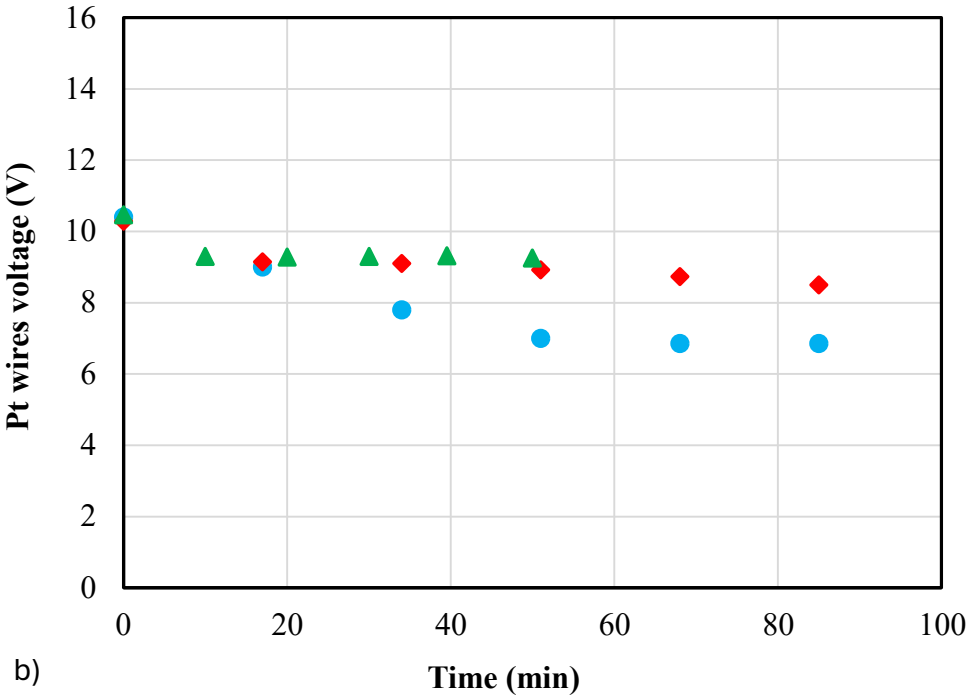

b)

788

789 **Figure S3**. Voltage at the Pt wires as a function of operation time for the three tested solutions for (a) layout
790 1 and (b) layout 2.

791

792

793